Gerrell Dabbs & Chrysanthe Preza

Noise Analysis for Hyperspectral Unmixing

Faculty Sponsor

Dr. Chrysanthe Preza

Abstract

Hyperspectral Imaging is a three-dimensional imaging technique which collects information from the electromagnetic spectrum. Hyperspectral images contain spectral signatures allowing for material identification and classification, making it useful for many fields. Hyperspectral imaging sees use in anomaly detection where there are several pipelines to utilize the imaging technique. An issue with these pipelines is their lack of generality, but a former graduate student of the CIRL successfully created a more general pipeline. Like others, their pipeline was created specifically for anomaly detection. However, there is interest in how it performs in purely noisy hyperspectral unmixing. In our investigation of the pipeline's behavior in this task, we find that the Sobel Operator would create solid color abundance maps which would cause a loss of information. As such, the operator was replaced with sharpening with varying degrees of success. However, there is still a need for a general solution.

Introduction

Images are indispensable in the sciences. They are a powerful tool when it comes to both representing and storing valuable information for different analytic tasks. The ability to store image data is also powerful as it allows for the analysis of scenes at both a different time and place than the original event recorded. By storing this information, we also can make use of computational techniques to extract features that would otherwise go unnoticed by the human eye. This field is known as image processing which is the act of performing different operations on images to analyze features in them. This includes the detection and enhancement of edges in an image, adjusting the contrast, and many other techniques. This can be seen in devices such as smartphones where it is responsible for our ability to search for information based on solely images or augmented reality, the act of superimposing objects onto reality using the camera on those devices.[6] Imaging processing sees further use in medical applications such as x-rays, or in surveillance, where people can be alerted of possible dangers. [4] Artificial intelligence makes use of imaging processing practices to effectively allow a computer to see the same way a human does in a field known as 'computer vision.' The proper utilization of image processing helps to streamline and improve daily life providing a permanent reason for the growth of the field.

The development of image processing requires understanding of the fact that not all images are the same in terms of data types. There are many applications of imaging processing that make use of standard RGB imaging which collects photos on the wavelengths of visible light and are the most typical data type when talking about an image. However, there exist other imaging methods which collect information over different wavelengths, including those which are not visible to the human eye. There are benefits to working with these other imaging types with a primary one being that they are more informative in some cases. Of these imaging types, we turn our attention to hyperspectral imaging, whihc is known for its ability to create information-dense datasets while allowing for the analysis and utilization of the special spectral properties for particular applications. These spectral properties allow for unique approaches to identifying what a scene contains while also doing so with a high degree of certainty than an imaging type such as standard RGB imaging cannot achieve. However, this does come at the cost of computational resources, with hyperspectral datasets being harder to handle. Despite this, it is worth working through the computational complexities and cost to utilize this imaging type.

Hyperspectral Imaging

Hyperspectral Imaging is an imaging technique which collects information from the electromagnetic spectrum rather than the visible light spectrum. This technique creates three-dimensional data by taking photos on the 'x' and 'y' axes at several different wavelengths denoted by 'λ'. The collection of photos is then 'stacked' on top of one another to create a 'data cube', a 3-dimensional representation of the data. In a hyperspectral image, pixel values represent reflectance which is the amount of light captured by the hyperspectral sensor at a given wavelength. While reflectance values are like color values or intensity values in visible light and grayscale images respectively, the analysis of reflectance values yields more information for identification when compared to the pixel value types.

Each unique material, or endmember, has a unique reflectance value across wavelengths known as a spectral signature. As this spectral signature is unique, there exists a particular spectral signature for each material that can be used to identify them, therefore making it possible to identify objects in a scene given there exists an acceptable ground truth or reference point for a material's spectral signature. For this reason, hyperspectral imaging is more practical than visible light imaging in applications focused on identification and classification.

Notably, there exists a similar imaging technique known as multispectral imaging. Multispectral imaging makes use of a similar concept to hyperspectral imaging in the sense that it is imaging over additional wavelengths as compared to just the visible light spectrum. However, hyperspectral imaging is still over more wavelengths than multispectral imaging. While multispectral imaging suffers from its lower wavelength count, it additionally suffers a lower spectral resolution when compared to hyperspectral imaging.[3] For the previously stated reasons, hyperspectral imaging sees usage in many fields such as astronomy, chemistry, agriculture, medicine, and surveillance. An example of a medical application is its use for tissue analysis, where it can be used to analyze certain properties of tissue. Another medical application is the analysis of absorption spectra to find the concentration and oxygen saturation of hemoglobin allowing for the identification of cancer hallmarks. [2]

Hyperspectral Unmixing

While hyperspectral imaging is a powerful tool on its own, it does suffer from a particular limitation. To ensure the accuracy of reflectance values, it is important that each pixel contains only one endmember, making that pixel pure. Otherwise, a mixed pixel will have a mix of reflectance values

within it, making it difficult to determine the material of the pixel. In this case, there is a need to 'unmix' the pixel to retrieve the reflectance of each individual material. The process of recovering the reflectance values is known as Hyperspectral Unmixing.

There are two approaches to unmixing: Linear and Nonlinear. Nonlinear is a more complex process, so linear unmixing will be used for an explanation. In the case of linear unmixing, the goal is to recover a linear combination of the endmembers which means that the coefficient of each endmember must be found. These coefficients represent the weighing of each endmember in a given pixel. If a pixel is pure, then the linear combination should be only one endmember with a coefficient of 1. If a pixel is mixed, then it should contain a noteworthy term for each endmember in the pixel with the coefficient for endmembers not contained in the pixel being 0 and therefore not affecting the pixel.

To perform hyperspectral unmixing, several algorithms are employed. Some of these hyperspectral unmixing algorithms are pixel purity index (PPI), fast iterative pixel purity index (FIPPI), and N-finder (N-FINDR). These algorithms exist to perform endmember extraction. It is important to understand that each algorithm performs differently in different cases so there is not a single best algorithm for general use. When unmixing, it is useful to have a visualization of the data. As such, there is a photo generated when unmixing known as an abundance map. An abundance map is a color scored image where the color at a given pixel indicates how much of a given endmember is contained at that pixel. This can be seen in Figure 1 where the warmer the color at a given pixel, the more that the material the abundance map is tracking is present in that pixel. For example, the third abundance map is tracking where there is water in the scene. The body of water is warm colored in the abundance map, showing that those pixels contain water. In the other abundance maps, the area where there was water in the third abundance map has a cool color, showing there is little to no water in those pixels.

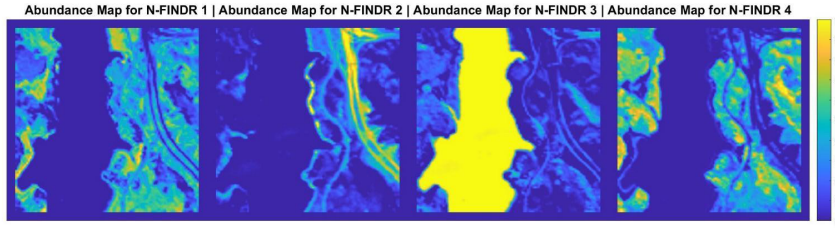

Figure 1.
Abundance Map Visualization

Focus of Study

This study is based on anomaly detection and a pipeline created for its enhancement when using hyperspectral processing techniques. Anomaly Detection refers to the process of finding outliers in a dataset and in the case of imaging, this would be to find out of place items. As described earlier, hyperspectral imaging allows for classification and identification of objects in a scene without the need for prior knowledge other than spectral signatures. As such, it is a powerful tool for the task and any advancements would help greatly in the field of surveillance.

The pipeline stems from a study conducted by a former graduate student in the CIRL [7]. The goal of his study was to create a pipeline that would improve hyperspectral anomaly detection along with outperforming pre-existing methods. The reason for this is due to the lack of generality in existing approaches to anomaly detections. Before his own contributions, pipelines either made a gaussian assumption, which assumed that anomalies were small and infrequent, or were computationally expensive with memory being noted as the main resource.[7] The student's method was an ensemble allowing for individual parts to be modified to produce better results. The parts of the method were band selection, gaussian blurring, and Sobel edge enhancements. This pipeline was successful in producing better results for anomaly detection, but it highlighted additional aspects to analyze such as the effect of different paint types on endmember extraction and how wrapped objects interact with the pipeline.

While there were different ideas to explore, there was one area of interest: noisy unmixing. The graduate student's pipeline had the goal of enhancing hyperspectral anomaly detection. The pipeline was not made with solely hyperspectral unmixing nor unmixing in noisy settings, but it makes mention of the importance of reducing noise. Noise naturally exists in hyperspectral images due to the resolution, but most popular datasets

have a reasonable level of it making it acceptable for hyperspectral tasks and testing. Simulating additional noise in these popular datasets would allow for an analysis of the pipeline under noise in a controlled and systematic way. As such, we had the goal of investigating if and how the pipeline handles noise and finding improvements in the case that it could not.

Testing the Original Pipeline

For our study, we used two known hyperspectral datasets. The first dataset is a popular dataset known as Jasper Ridge. The version of the dataset we are using is a 100 x 100 subset recorded at 198 wavelengths making the dimensions 100 x 100 x 198. It is known that there are 4 endmembers: Tree, Soil, Water, and Road. A representation of the dataset can be seen in Figure 2.

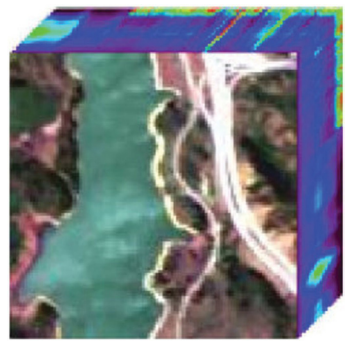

Figure 2.
Jasper Ridge Data Cube Visualization [5]

The second dataset is known as Cuprite, a picture of multiple minerals. The image is a 250 x 190 region recorded at 224 wavelengths making the dimensions 250 x 190 x 224. There are 14 endmembers, each a different mineral. However, an endmember count of 12 is accepted due to similarities between minerals. A representation of the dataset can be seen in Figure 3.

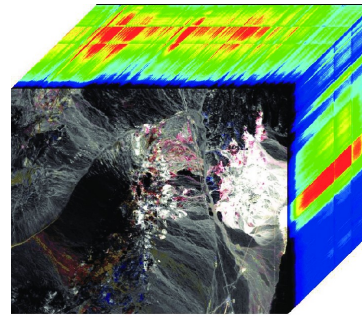

Figure 3.
Cuprite Data Cube Visualization [1]

Another factor to note is that some datasets have ground truths. A ground truth is simply an additional piece of data which indicates the absolutes of the dataset. It will inform the user what material each endmember is, the reflectance values at each wavelength, and the correct abundance map for each endmember. Furthermore, ground truths are split into a file for the abundance maps and a file for the reflectance values or endmembers. Jasper Ridge has an abundance map for both the reflectance values and abundance maps, but the file format for the abundance maps is not possible to work with for easy comparison. Cuprite has a ground truth for reflectance values, but not for its abundance maps. This makes it impossible to compare any experimental data related to abundance maps to absolute information. Additionally, any oddities with abundance maps from this dataset would not be apparent due to this missing data. The lack of ground truths is not a rare occurrence in Hyperspectral Imaging as it is not easy to produce ground truth data.

As noise is an integral part of our study, it must be quantified in some manner. Our metric for noise is known as Signal-to-noise ratio or, as it will be referred to, SNR. The higher the SNR, the lower the noise. It is worth noting that there exists some amount of noise naturally in experimental data, especially due to the resolution of hyperspectral sensors. As such, even when only a little noise is simulated, there will still exist noise from the original dataset. Nevertheless, we will treat the original dataset before noise simulation as the ‘noiseless’ dataset. The simulation and addition of noise was conducted through a user-defined MATLAB function which uses the pixel values in the image to generate an array of random numbers scaled to an input value with the same dimensions as the image to add to the image to create a noisy image.

Additionally, as we want to determine the impact of noise, we must use additional metrics. There are two metrics of value for this kind of study, Mean-Squared Error, which will be referred to as MSE, and Structural Similarity Index Measure, which will be referred to as SSIM. In imaging, MSE calculates the error between two images while SSIM calculates the similarity between same position pixels in two images. When it comes to evaluation of performance, the goal is to minimize the value of MSE while maximizing the value of SSIM. In MATLAB, there are built-in commands for the acquisition of these metrics. This is to say that MSE and SSIM values will be calculated between the noiseless abundance map for each endmember and their noisy counterparts at the different SNR values. This will allow us to see how similar the noisy processed results are to the noiseless ones.

To establish a starting point, the two datasets were passed through the pipeline so that the metrics could be computed. In all cases, the MSE and SSIM metrics were computed between the noiseless and noisy abundance maps of the given dataset.

Jasper	MSE					
SNR (dB)	22.35	24.57	26.61	29.62	35.64	38.65
1: Soil	4.270E-02	3.560E-02	2.940E-02	2.780E-02	1.880E-02	1.820E-02
2: Road	2.290E-02	2.240E-02	2.370E-02	1.890E-02	2.000E-02	2.230E-02
3: Water	5.000E-02	4.370E-02	3.220E-02	3.180E-02	2.390E-02	2.590E-02
4: Tree	2.540E-02	2.080E-02	1.670E-02	1.590E-02	1.390E-02	1.370E-02

Table 1.
Jasper Ridge (Original Pipeline),
MSEs for Individual Endmember #1-#4

In the case of the Jasper Ridge data, a few things can be noted (Table 1). On average, the endmember with the lowest MSE was the tree endmember, followed by the road, soil, and then water. The two highest MSE endmembers also see a large jump in their MSE values as the SNR decreases.

Jasper	SSIM					
SNR (dB)	22.35	24.57	26.61	29.62	35.64	38.65
1: Soil	8.70%	10.95%	13.06%	16.33%	22.55%	35.30%
2: Road	40.25%	43.21%	47.67%	48.79%	53.68%	48.22%
3: Water	36.72%	36.51%	40.85%	37.45%	43.46%	43.99%
4: Tree	18.67%	23.06%	38.02%	27.32%	36.34%	51.60%

Table 2.
Jasper Ridge (Original Pipeline),
SSIMS for Individual Endmembers #1-#4

Viewing **Table 2**, it can be seen that SSIM differs from MSE with the highest SSIM obtained for the road. Additionally, the tree and soil have the greatest change in their SSIM values at the highest SNR to the lowest SNR. With some exceptions, the increase of SNR results in the decrease of MSE and the increase of SSIM with the opposite also being true.

Cuprite	MSE					
SNR (dB)	27.44	30.45	33.46	36.47	39.48	42.49
1	9.917E-03	1.521E-02	8.152E-03	9.360E-03	7.187E-03	3.904E-02
2	1.894E-02	2.114E-02	1.904E-02	3.157E-02	2.549E-02	2.929E-02
3	1.459E-02	2.403E-02	1.529E-02	1.317E-02	1.818E-02	3.279E-02
4	7.757E-03	8.742E-03	1.697E-02	1.232E-02	1.049E-02	9.807E-03
5	2.922E-02	2.547E-02	2.603E-02	2.921E-02	2.676E-02	3.193E-02
6	2.017E-02	2.308E-02	2.275E-02	2.445E-02	2.002E-02	3.101E-02
7	4.922E-03	4.251E-03	5.705E-03	1.813E-02	3.861E-03	2.817E-02
8	2.135E-02	2.237E-02	2.541E-02	2.706E-02	3.045E-02	3.784E-02
9	2.128E-02	1.980E-02	2.495E-02	3.993E-02	2.191E-02	3.549E-02
10	5.497E-02	5.212E-02	5.032E-02	5.738E-02	5.319E-02	8.153E-02
11	4.583E-02	4.739E-02	4.548E-02	5.003E-02	4.975E-02	8.037E-02
12	4.151E-02	4.059E-02	6.239E-02	5.488E-02	4.407E-02	6.582E-02

Table 3.
Cuprite (Original Pipeline),
MSE for Individual Endmembers #1-#12

Cuprite	SSIM					
SNR (dB)	27.44	30.45	33.46	36.47	39.48	42.49
1	10.47%	9.14%	36.07%	39.54%	43.07%	23.36%
2	7.79%	6.78%	14.41%	9.11%	6.14%	7.60%
3	7.24%	6.26%	22.07%	25.88%	20.09%	6.67%
4	23.79%	30.38%	7.68%	26.15%	24.19%	23.97%
5	5.09%	17.42%	15.88%	11.04%	22.84%	3.94%
6	15.31%	11.99%	11.87%	9.76%	14.78%	7.75%
7	34.70%	40.92%	33.98%	30.85%	41.95%	13.28%
8	11.97%	19.23%	15.84%	11.32%	17.44%	5.42%
9	8.61%	20.16%	18.42%	2.90%	20.54%	10.73%
10	10.50%	5.97%	15.30%	18.72%	20.16%	8.38%
11	5.74%	6.13%	6.10%	5.25%	6.47%	1.70%
12	4.07%	4.24%	1.02%	1.87%	3.48%	1.21%

Table 4.
Cuprite (Original Pipeline),
SSIMS for Individual Endmembers #1-#12

When using the pipeline on Cuprite (Tables 3 and 4), endmembers are not labeled by their material as there does not exist a ground truth for the abundance maps. Cuprite also has a sizable number of endmembers, so lacking the ground truth makes it hard to extract data by inspecting the values of MSE and SSIM. Due to the large endmember count, it is helpful to take the MSE values for each endmember at a given SNR value and sum them together to create a sum of MSE Values for each SNR value resulting in a sum of errors that will be referred to as 'Sum MSE'. For SSIM, we can take an average of the SSIM values for each endmember at a given SNR value to create an average similarity value that shall be referred to as 'Average SSIM'. By doing this, it is easier to observe the effect of noise on the metrics without having to look through each individual endmember.

SNR (dB)	Sum MSE	Average SSIM
27.44	2.905E-01	12.11%
30.45	3.042E-01	14.89%
33.46	3.225E-01	16.55%
36.47	3.675E-01	16.03%
39.48	3.114E-01	20.10%
42.49	5.031E-01	9.50%

Table 5.
Cuprite (Original Pipeline),
Summed MSE and Averaged SSIM

Condensing the data into sums and averages, as seen in Table 5, makes it clear that the behavior of the pipeline on Cuprite is similar to its behavior on Jasper Ridge with the main difference being that the highest SNR's results are not better than the results at the lower SNRs. We once again see that an increase in SNR results in a decrease in MSE and an increase in SSIM.

When running the pipeline on these datasets, it was determined that Sobel Operation did not work as its inclusion would result in the generation of solid color abundance maps, meaning that the maps were indicating that the scene consisted of entirely one endmember, and therefore rendering the abundance maps useless. This was confirmed as when removing it, abundance maps returned to normal. As such, the Sobel Operator was removed. However, the removal of the Sobel operation leaves out a valuable part of the pipeline, calling for a need to replace it. To try to remedy this, sharpening was implemented in its place by creating a sharpening mask or matrix to then apply to the image. Sharpening performs a similar action to Sobel-Edge Enhancements while it avoids producing solid color abundance maps.

Testing the Modified Pipeline

The testing for the modified pipeline is the same as for the original pipeline.

Jasper	MSE					
SNR (dB)	22.35	24.57	26.61	29.62	35.64	38.65
1: Soil	4.990E-02	4.010E-02	3.060E-02	2.780E-02	1.320E-02	1.370E-02
2: Road	2.540E-02	2.160E-02	2.070E-02	1.530E-02	1.360E-02	1.520E-02
3: Water	4.940E-02	3.970E-02	2.930E-02	2.610E-02	1.830E-02	2.040E-02
4: Tree	3.250E-02	2.040E-02	1.450E-02	1.210E-02	8.300E-03	8.600E-03

Table 6.
Jasper Ridge (Modified Pipeline),
Individual Endmember MSEs

The modification to the pipeline causes Jasper Ridge's endmembers to have lower MSE numbers at higher SNR values (Table 6). For 38.65 dB and 35.64 dB, each endmember sees a minimum of a 21% decrease in MSE with some seeing 30% or greater. At 29.62 dB, the soil does not benefit while the others see a decrease of at least 18%. However, at lower SNR values, there is an increase in MSE in the modified pipeline compared to the original pipeline. For 24.57 dB, the soil sees a 13% increase in MSE while the others still see slight decreases. At 22.35 dB, only water decreases by 1% while the others increase by at least 11%.

Jasper	SSIM					
SNR (dB)	22.35	24.57	26.61	29.62	35.64	38.65
1: Soil	17.12%	26.16%	32.73%	37.77%	54.44%	64.83%
2: Road	32.28%	46.31%	49.10%	57.44%	66.59%	72.49%
3: Water	27.80%	42.27%	38.42%	41.57%	55.01%	59.46%
4: Tree	34.16%	42.27%	47.41%	50.78%	60.47%	76.06%

Table 7.
Results from Jasper Ridge (Modified Pipeline),
Individual Endmember SSIM

For SSIM (Table 7), the results are similar to MSE. At 38.65 dB and 35.64 dB, there is a minimum increase of 17% and 1%. All other SNR values see a decrease in either one or two endmembers. From 29.62 dB, soil always performs worse, starting with a 23% decrease in SSIM and reaching a 57% decrease at 22.35 dB. The road endmember also does worse, but only at 22.35 dB. The water and tree endmembers always see an increase in SSIM.

Cuprite	MSE					
SNR (dB)	27.44	30.45	33.46	36.47	39.48	42.49
1	5.039E-02	4.965E-02	2.730E-02	1.866E-02	1.266E-02	1.134E-02
2	1.910E-02	3.858E-02	3.784E-02	7.321E-02	4.941E-02	7.420E-02
3	1.801E-02	4.093E-02	5.173E-02	3.505E-02	7.720E-02	4.067E-02
4	1.740E-02	7.959E-03	2.269E-02	1.650E-02	1.002E-02	5.220E-02
5	3.090E-02	3.484E-02	7.552E-02	2.906E-02	1.097E-02	3.754E-02
6	2.022E-02	1.505E-02	1.822E-02	4.091E-02	3.890E-02	2.178E-02
7	3.102E-02	1.660E-02	3.528E-02	2.984E-02	8.615E-03	5.177E-03
8	3.391E-02	2.014E-02	1.345E-02	3.621E-02	1.908E-02	5.154E-02
9	2.869E-02	2.014E-02	3.027E-02	7.916E-02	3.492E-02	3.856E-02
10	4.596E-02	4.338E-02	3.252E-02	7.941E-02	9.119E-02	5.043E-02
11	4.169E-02	3.864E-02	1.130E-01	1.162E-01	5.172E-02	2.750E-02
12	2.409E-02	8.129E-02	3.046E-02	3.523E-02	3.004E-02	3.468E-02

Table 8.
Results from Cuprite (Modified Pipeline),
MSEs for Individual Endmember #1-#12

Cuprite	SSIM					
SNR (dB)	27.44	30.45	33.46	36.47	39.48	42.49
1	0.99%	1.56%	0.10%	3.09%	15.68%	6.18%
2	30.90%	13.97%	14.60%	-17.75%	-13.33%	12.54%
3	29.10%	23.81%	23.98%	36.90%	-8.23%	34.13%
4	15.72%	43.11%	4.16%	8.61%	29.07%	1.40%
5	19.10%	5.32%	-10.72%	25.26%	59.54%	12.25%
6	27.66%	52.45%	50.51%	-6.38%	0.16%	40.53%
7	-2.78%	5.44%	-0.54%	15.18%	21.91%	38.00%
8	-0.29%	40.70%	41.20%	3.84%	51.77%	-8.58%
9	39.92%	47.23%	12.57%	-9.27%	43.25%	33.16%
10	35.36%	31.61%	45.12%	16.10%	9.81%	39.25%
11	45.52%	43.30%	-4.61%	-5.51%	50.69%	53.10%
12	64.29%	-7.24%	47.29%	63.03%	58.07%	47.57%

Table 9.
Results from Cuprite (Modified Pipeline),
SSIMs for Individual Endmember #1-#12

For Cuprite (Tables 8 and 9), there is ample variance in the behavior at different SNRs. We use the same idea from earlier and condense our data into sums of errors and averages of similarities.

SNR (dB)	Sum MSE	Average SSIM
27.44	3.614E-01	25.46%
30.45	4.072E-01	25.11%
33.46	4.883E-01	18.64%
36.47	5.895E-01	11.09%
39.48	4.347E-01	26.53%
42.49	4.456E-01	25.79%

Table 10.
Results from Cuprite (Modified Pipeline),
Summed MSE and Average SSIM

In Cuprite (Table 10), the MSE increases by at least 24% for all SNR besides 42.49 dB. At that SNR, there is an 11% decrease in MSE. SSIM

also increases at all SNRs except for 36.47 dB where it sees a 31% decrease. For all others, it sees at least a 13% increase and at most a 171% increase at 42.49 dB.

Discussion

As the data displays, there are improvements in SSIM and MSE at higher SNRs while lower SNRs see worsening results. This goes back to the graduate student's point on generalization and how it is a common problem among anomaly detection pipelines. There are two focus points when looking at the data and considering further questions: The Sobel Operator and the endmembers that only saw benefits from sharpening.

The Sobel Operator works by convolving the image with different matrices to determine where there is a sharp change in pixel values and therefore an edge. By adding simulated noise in random places in the scene, sharp changes exist at more points than just object edges. This results in the addition of extra edges in the scene. This is likely why solid color abundance maps were produced whenever the Sobel Operator was used on the scene. Another issue with removing the Sobel Operator is that it removes an additional layer of smoothing done by the operator itself.

The endmembers that only saw an improvement from sharpening are the water endmember for both MSE and SSIM, and the tree endmember only for SSIM. These are both endmembers which have many connected parts throughout the scene with water being one large body, and the tree being four sizable parts opposed to the scattered nature of the soil or the small road. It is notable that the road endmember in Jasper Ridge performed well at all SNRs except for the lowest, and that the road is comprised of roughly 3 pieces. This may indicate that the main issue in noisy unmixing arises from the inability to clearly define edges in the same way the Sobel Operator is likely to enhance the noise as stated prior.

The lack of generalization A possible solution to the issue is to investigate general denoising for hyperspectral imaging. One common approach to the need for denoising is found in machine learning and artificial intelligence where different models can be constructed. These methods can be either model-based or learning-based with both having their own requirements to work with.[8] In further study, this may yield the best result.

Conclusion

Imaging a prevalent tool in many fields yields useful information. Hyperspectral Imaging is an imaging method capable of creating informa-

tion-dense datasets compared to other methods such as RGB or visible light imaging. Due to the nature of hyperspectral imaging, it is also prevalent in anomaly detection where many pipelines make assumptions about a scene to produce results. In prior work, a pipeline was created that was able to produce better results in generalized settings unlike pipelines of the time. While the pipeline succeeded in its immediate goal, there was interest in how it performed in purely unmixing particularly cases with noise. To test this, noise was simulated through MATLAB commands. Testing revealed that the Sobel Operator did not respond well to noise but could be removed to process images regardless. The removal of the operator created a need for a sufficient replacement and for that sharpening was tried. Sharpening was able to improve some cases, but did not generalize causing a return to the original issue stated in the former graduate student's study. The pipelines prior to their contribution made assumptions about the given data to enhance the task at hand. However, these assumptions hurt the generality of the pipelines, resulting in varying results across different datasets. As there is a need for a more general solution, an approach to solving this problem could be found in the domain of machine learning and artificial intelligence models that are able to adapt based on the given dataset.

Acknowledgement

I would like to thank the Helen Hardin Honors College for enabling me to do research through their Summer Fellowship. I also would like to thank Dr. Chrysanthe Preza for being my research advisor and allowing me this opportunity.

References

[1] Kaya, S. (2017). A comparative analysis of classification methods for hyperspectral images generated with conventional dimension reduction methods.

[2] Lu, G., & Fei, B. (2014). Medical hyperspectral imaging: a review. *Journal of biomedical optics*, *19* (1), 10901. https://doi.org/10.1117/1.JBO.19.1.010901

[3] Niu, B., Feng, Q., Chen, B., Ou, C., Liu, Y., & Yang, J. (2022). HSI-TransUNet: A transformer based semantic segmentation model for crop mapping from UAV hyperspectral imagery. *Computers and Electronics in Agriculture*, *201*, 107297. doi:10.1016/j.compag.2022.107297

[4] Sharma, P., & Singh, R. (2022). *Application of Image Processing in Real World*.

[5] Song, D., Sun, N., Xu, M., Wang, B., & Zhang, L. (2020). Fast Unmixing of Noisy Hyperspectral Images Based on Vertex Component Analysis and Singular Spectrum Analysis Algorithms. *Canadian Journal of Remote Sensing*, *46*, 1–15. doi:10.1080/07038992.2020.1726735

[6] Thabet, R., Mahmoudi, R. & Bedoui, M.H. (2014). Image processing on mobile devices: An overview. doi:10.1109/IPAS.2014.7043267

[7] Younis, M. (2023) "Investigation of hyperspectral data unmixing and its impact on the task of anomaly detection." *Electronic Theses and Dissertations*. 3343. https://digitalcommons.memphis.edu/etd/3343

[8] Zhang, T., Fu, Y. & Zhang, J. (2022). Guided Hyperspectral Image Denoising with Realistic Data. *Int J Comput Vis, 130*, 2885–2901. https://doi.org/10.1007/s11263-022-01660-2